ACS APPLIED POLYMER MATERIALS

Article

Cite This: ACS Appl. Polym. Mater. 2019, 1, 2525−2534

pubs.acs.org/acsapm

Wet-Stacking Lamination of Multilayer Mechanically Fibrillated Cellulose Nanofibril (CNF) Sheets with Increased Mechanical Performance for Use in High-Strength and Lightweight Structural and Packaging Applications

Sami M. El Awad Azrak,[†] Caitlyn M. Clarkson,[†] Robert J. Moon,[‡] Gregory T. Schueneman,[‡] and Jeffrey P. Youngblood*[,†]

[†]School of Materials Engineering, Purdue University, West Lafayette, Indiana 47907, United States of America

[‡]Forest Products Laboratory, United States Forest Service, Madison, Wisconsin 53726, United States of America

Supporting Information

ABSTRACT: Mechanically fibrillated cellulose nanofibril (CNF) sheets of varying thicknesses were fabricated by using a wet stacking lamination technique without the use of solvents other than water or binders. The use of this technique allowed for the creation of multilayer structures with a working area of 117 mm by 117 mm and thickness of up to 0.547 ± 0.03 mm in under 2 h, which represents the shortest total processing time reported for such thickness of CNF sheets. To highlight the capabilities of utilizing wet stacking, the thickest reported 100% pure multilayer CNF sheet with a thickness of 1.65 ± 0.02 mm was produced. To gauge the effect of processing parameters on the mechanical performance of the produced sheets, thickness (85−547 μm thick), pressing time (35 min, 1 h, and 2 h), pressing pressure (0−5.17 MPa), and loading rate (4 min, 2 min, and 20 s) were varied. Tensile testing results show that the ultimate strength increased as the thickness increased and subsequently reached a plateau at a value of 207 ± 2.51 MPa at a critical thickness between 85 ± 2 and 153 ± 4 μm. A slight decrease in ultimate strength to a value of 184 ± 10.9 MPa was seen for the thicker 547 μm (0.547 mm) specimens. The specific strength was comparable to 2024 aluminum (T3 tempered) due to the relatively low density of CNF. The apparent toughness (work of failure) of the sheets was found to be on average 3.53 ± 0.36 MJ/m^3, which is about 6 times greater than the reported value for poly(styrene). Because of their improved mechanical properties, these sheets could serve in high-strength and low-density structural applications where aluminum alloys (2024 and 6061) and packing materials/containers where commodity polymers like poly(styrene) are currently used.

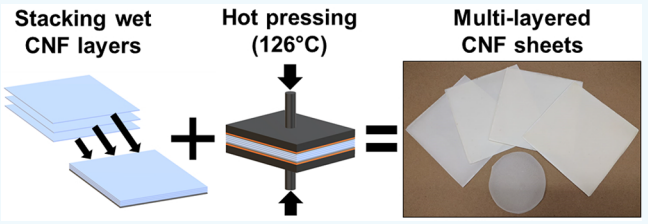

KEYWORDS: *nanocellulose, wet stacking, CNF lamination, CNF sheets, CNF laminate*

INTRODUCTION

Ever since bleached cellulose pulp was first fibrillated, the extracted cellulose nanofibrils (CNF) have become a very attractive material to reinforce, replace, or reduce the need of oil-derived synthetic polymers.[1,2] This is largely due to the inherent sustainability and abundance of cellulose in nature as it can be harvested from many sources like wood, plants, algae, and even bacteria.[3] The extracted nanofibrils boast high crystalline contents (from 27% to >80%, depending on the source) and increased surface area with large aspect ratios (L/D = 5−500) and can easily form hydrogen bonds with other surrounding fibers through native hydroxyl groups.[3] Within CNF types, mechanically fibrillated cellulose nanofibrils (CNF) are larger and more aggregated than the chemically treated TEMPO oxidized cellulose nanofibrils (TOCNF), giving them a white appearance in the aqueous dispersion state, as opposed to the translucency/clarity of TOCNF.[4−7] Many researchers have utilized these facts and have incorporated or fabricated into films, fibers, and nanocomposites, all of which attain impressive properties when compared to standard commodity polymers.[3,8] For example, cellulose nanocrystals (CNCs) have been reported in coatings for packing applications as well as a reinforcement phase in nanocomposites.[9−13] On the other hand, because of their larger size, CNF are more readily formed into larger structures such as self-standing neat isotropic films. For example, CNF films can attain impressive mechanical properties with reported values of ultimate strength reaching 232 ± 19 MPa and a tensile elastic modulus of 13.4 ± 0.25 GPa.[14] Yet, the formation of such films is time-consuming due to the required water removal which largely depends on the thickness of the produced films.[14]

Received: July 8, 2019
Accepted: August 15, 2019
Published: August 15, 2019

DOI: 10.1021/acsapm.9b00635
ACS Appl. Polym. Mater. 2019, 1, 2525−2534

For CNF, the film making process often starts with a slurry (0.1−3 wt % in water) which is evenly dispersed using shear mixers and/or sonicators. The mixture is then poured in a mold or reservoir where the solvent (usually water) is removed and the web consolidates at the bottom. The total film processing time varies based on the method used to remove the solvent and ranges from roughly an hour for hot pressing operations up to a couple of weeks for controlled room temperature evaporation. Moreover, depending on the mold/reservoir dimensions, the variety of processing methods can yield different size films. For example, those films produced by using solution casting and evaporation techniques rely on the use of standard Petri dishes with a 90 mm diameter. On the other hand, the thickness of the films can be controlled by the amount of slurry initially added in the mold. Standard thicknesses reported for neat CNF films range from 0.033 mm (33 μm) to 0.08 mm (80 μm).[15−17] However, thickness is practically limited by cracking and curling during evaporation due to residual stresses and the long evaporation/filtration time required to consolidate and dry the films which requires free water to escape through the dense fibrillar network as the escape path becomes increasingly tortuous due to the formation of fiber−fiber hydrogen bonds and humidity gradients.[18,19] For example, it takes roughly 45 min to filter CNF slurry through a 0.65 μm pore size membrane to create a film with a final thickness of 0.06 mm.[14] This problem is well-known in established industries such as papermaking, where evaporation rates are fastest during the initial sheet farming step and then significantly decrease during the later stages of drying where extensive structural changes occur to the web.[20,21] As processing time increases with thickness, this presents a challenge for the creation of thicker CNF sheets or plaques which could serve as structural and other packaging materials. One solution for creating thicker nanocellulose structures (0.1 to 3.2 mm) without significantly increasing processing time is to create polymer nanocomposites. In these structures a polymer matrix is often used, and cellulosic nanomaterials (CN) will be added as the reinforcing phase. Two major drawbacks of using composite systems to make thicker structures is the poor compatibility between the different phases and the low dispersibility of the hydrophilic material (CN) in a highly hydrophobic matrix. This often limits the amount of material that can be added or dispersed, leading to peak composite performance at relatively low solids loadings (<10 wt %) of CN due to particle aggregation. Additionally, low solids loading also defeats the initial goal of reducing the dependence on oil-derived polymers. Thus, there is still a need to find a better way to process thicker CN structures and study their mechanical properties.

In this work, a four-step wet stacking technique was developed and used for the creation of multilayer CNF sheets with varying thicknesses and without the use of additional solvents or binders. Wet stacking allowed increased thickness of the CNF sheets without significantly increasing total processing time which represents a significant advantage over other conventional film making processes. Additionally, the use of this technique allowed for the creation of the thickest reported pure multilayer CNF sheet with a working area of 117 mm by 117 mm and thickness of 1.65 ± 0.02 mm. The effect of thickness on the mechanical performance of the sheets was investigated by varying the number of stacked CNF layers from 1 to 8 layers thick. The results were contrasted with commodity polymers commonly used for packing applications and metals used in structural applications like poly(styrene), nylon-6,6, Al 2024, and Al 6061. The pressing time, pressing pressure, and loading rate were varied to gauge their effect on the mechanical performance of the produced sheets. To elucidate why thicker sheets performed better than the thinner ones, SEM photomicrography was utilized to view the cross-sectional area of the sheets as well as the fracture surface.

EXPERIMENTAL SECTION

Materials. The 5-gallon buckets of CNF from Kraft pulp were bought directly from University of Maine, Orono, ME (batch #98; 3 wt % CNF−water slurry; 90% fines). These fibrils had a mean diameter of 38 nm as taken from a transmission electron microscopy image (see Figure S1). Over 15 particle diameters were measured using an open source software (ImageJ). The material was used as delivered and diluted to 1 wt % with deionized water. The process of making the cellulose slurry is explained more in detail by de Assis et al.[5]

The materials used for building the dewatering frame were as follows: two stainless steel filtering wire cloths/sieves ("Dutch weave", 316SS) with a mesh size of 165 × 1400; one filter felt (polyester) with a 10 μm pore size; one polyurethane superabsorbing foam/sponge (Aquazone); perforated staggered hole 0.635 cm thick PVC sheet (50% open area and 1.27 cm hole diameter); and four 5 × 10 cm^2 wood studs cut to a length of 40.64 cm. A wooden frame was constructed to hold the perforated PVC sheet. The filter felt was then laid on top of the PVC sheet, followed by the metal filter mesh (Figure S2). The total dewatering frame working area is 929 cm^2 (W × L = 30.48 × 30.48 cm^2). Additionally, aluminum 2024 (T3 tempered), aluminum 6061 (T6 tempered), poly(styrene), and nylon-6,6 sheets were bought to use as comparison materials. All materials were bought directly from McMaster Carr Supply Company, Elmhurst, IL, with exception of the wood studs which were sourced in-house.

Preparation of CNF Sheets. For all case studies, the initial CNF concentration of 3 wt % was diluted to 1 wt % by adding deionized (DI) water at a ratio of 1 to 2 (CNF to water). To make a single layer, 300 g of CNF slurry (at 3 wt %) and 600 g of DI water were added into a larger plastic container and vigorously mixed by hand for 3−4 min. The contents were then poured in a zigzag fashion over the metal filtering mesh which was placed inside the frame. The frame and mixture were slightly shaken to make sure that the CNF slurry was evenly distributed across the surface of the filtering mesh. A second metal filter mesh was then carefully laid on top of the CNF slurry followed by the sponge. The slurry remained in the frame for 10 min to allow for filtration by gravity and capillary suction to occur. To aid capillary suction, evenly distributed pressure was then applied to the sponge by using a painter roller in a rowing fashion for 10 min. When the sponge was completely soaked, it was squeezed and placed back on top of the filtering mesh where the pressure was applied a second time. This process was repeated as needed until no more water was extracted by the sponge. The CNF web, now consolidated to ∼7 wt %, was removed from the frame and carried between the two metal meshes. The CNF sandwich was then passed through a 30.48 cm wide, tabletop slip roller (WFSR1.0) seven times. The rolling gap width was decreased slightly after each pass to gradually apply more pressure to the web and further increase the solids loading of the CNF web. After rolling, the solids loading reached ∼10 wt %, and the CNF web was capable of being separated from the meshes by hand. Large films with an initial area of 30.48 × 30.48 cm were sectioned into four smaller sections (15.24 × 15.24 cm^2). These smaller sections were stacked, and the sides were trimmed to a final sheet area of 11.7 × 11.7 cm^2. Finally, the stacked layers were hot pressed at a temperature of 126 °C until dry (∼99 wt %) for different pressing times (35 min, 1 h, and 2 h) by using a hydraulic heated laboratory press model No. 3690 (Carver). The final thickness of the sheet is dependent on the number of layers stacked before the final hot-pressing step. Figures S3 and S4 portray each step in this process while Figure S2 shows a graphical illustration of the major steps taken. Step 2 in the process is

DOI: 10.1021/acsapm.9b00635
ACS Appl. Polym. Mater. 2019, 1, 2525−2534

optional, yet it was incorporated to further reduce the water content of the layers as the heated press used in the final step did not have any drainage system for liquid water. Moreover, the initial press filtration step could be performed by other means instead of gravity and capillarity (sponge) like vacuum pumps or mechanical presses, but this could represent a costlier and more complex route. The total solids concentrations were calculated by dividing the weight of the completely dry web by the weight of the wet web. The process outlined in Figures S2–S4 was used to produce pure multilayer CNF sheets of varying thicknesses (Figure 1a). The use of this technique

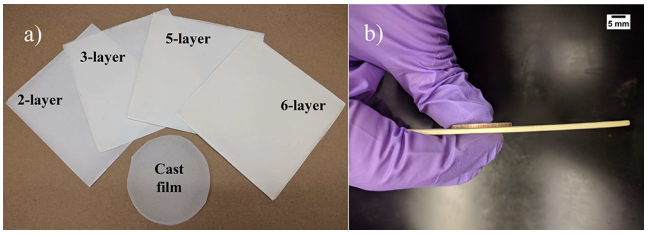

Figure 1. (a) Different thickness CNF sheets prepared by using the layer-by-layer wet stacking technique described in Figure S2. For comparison, a solution-cast CNF film (~90 mm diameter) is placed at the center. Note it becomes much harder to see through the sheets as the number of layers increased. (b) Cross section of the thickest reported pure multilayer CNF sheet ($t \sim 1.65$ mm); a US quarter is pressed against the surface for comparison.

allowed for the creation of the thickest reported pure multilayer CNF sheet with a working area of 117 mm by 117 mm and a thickness of 1.65 ± 0.02 mm made out of 24 layers of CNF (Figure 1b). Yet, thicker sheets could be made by stacking additional layers. Steps 1 and 2 (Figure S2) are very similar to the process used to create hand sheets of paper from hydrated paper pulp by using a sheet machine where a single large layer is formed and dried.[22]

Mechanical Properties and Density. Following ASTM D638 dogbone specimens were cut from prepared CNF sheets using a laser cutter PLS6MW MW (Universal Laser Systems) with a 10.6 CO_2 source and 2 MW optics. Several laser passes were needed to cut thicker samples. The tensile specimens were 92 mm long and had a neck width of 4.80 mm. After laser cutting, all the specimens were conditioned in a desiccator at 23% RH for at least 2 days before mechanical testing. An electromechanical testing machine (MTS Insight) was used for tensile testing of dogbone specimens with a 1000 N load cell and serrated film clamps. Sandpaper was added at the grips to avoid specimen slippage. The crosshead speed was set to 1 mm/min for all samples. All the samples were preloaded to 1 N. The ambient relative humidity could not be controlled and varied from 30% to 50% RH during mechanical testing, but large sample groups were tested together to reduce variation. The ultimate strength was taken to be the strength at failure. The Young's modulus was obtained by steepest slope method, and the strain was measured based on crosshead displacement (no extensometer was used); all the values were gathered from the built-in software (TestWorks 4). Grip compliance was measured by using a thick 1020 steel specimen and was subtracted from the results. The area under the stress versus strain curve was taken to be the apparent toughness or work of failure (MJ/m^3) of the specimen and was integrated using a built-in function in OriginPro. Density was measured on smaller square samples (8 mm by 8 mm) which were cut from the same sheet as the specimens. A micrometer and a caliper were used for measuring thickness and width while mass was measured with an analytical balance (VWR).

Scanning Electron Microscopy (SEM). CNF sheet surface texture, cross-sectional area, and fracture surfaces were imaged by using a Quanta 650 FEG field emission electron microscope. Prior to imaging, samples were secured to a conductive metal stub with copper and carbon tapes and then sputter-coated (SPI sputter-coater) with a platinum–gold target for 60 s. No polishing or sanding was used. Samples were imaged at 2–7 keV and spot size of 3–5. The working distance varied from 8 to 32 mm depending on whether sample topography or resolution was the objective. For the cross-sectional area analysis, a total surface length of 8 mm (i.e., the entire length of the density samples) was scanned before taking any SEM image.

Optical Profilometer. CNF sheet surface roughness was imaged using a Zygo Corporation (NewView 8000) optical profilometer. A 10× or 2.75× magnification was used for all the images taken. Because of the nonreflective nature of CNF, the studied samples were sputter-coated (SPI sputter-coater) with a platinum–gold target for 60 s. A cylindrical baseline/plane correction was applied to all captured surfaces from which the roughness values (*Sa*, *Sq*, and *Sz*) were automatically calculated.

Statistical Analysis. At least eight samples per CNF sheet were tested for each data point, and a minimum of 13 samples were tested to generate the baseline (one layer, 0 MPa); eight samples were tested of the 80 μm thick cast CNF film, which were depicted as dashed lines. For metal and commodity polymer specimens (Al 2024, Al 6061, poly(styrene), and nylon-6,6) at least three samples were tested. All specimens were visually inspected for excessive roughness or burn marks prior to testing. Only those with significant defects were removed from the analysis. Statistical analysis was done using OriginPro. A normality test was performed on all sample data sets to verify normal distribution. The error bars shown represent a single STD away from the mean. Student's t test with a 95% confidence interval was used to determine whether there was significant statistical difference/similarity between data sets. For the density versus ultimate strength analysis, residual analysis was utilized to remove any outliers which are highlighted in red. Data points with a standardized residual above or below ±10 STD were excluded from the linear fit.

RESULTS AND DISCUSSION

Sheet Processing Time and Surface Texture Analysis. A significant advantage of processing thicker CNF sheets in a wet stacking lamination approach (Figure S2) is the fact that dewatering time is not significantly increased. This is due to the ease at which water can escape through the thinner prestacked layers (steps 1 and 2, Figure S2) rather than a thicker CNF web (step 3, Figure S2). In this way, the pre-dewatered CNF layers (~10 wt %) are simply stacked on top on each other and hot pressed to form a final consolidated thicker structure. This differs from some of the most common techniques like solution casting and vacuum filtration plus hot drying, where the final thickness of the CNF sheet depends on the amount of material that was initially added into the reservoir for filtration and a thick CNF cake forms at the bottom. Table 1 compares two common processing techniques used to make CNF sheets with that of the wet stacking lamination approach. The total processing times are estimated based on laboratory trials and extrapolated from what has been

Table 1. Wet Stacking Lamination Approach Compared with Two Common CNF Film Processing Techniques

	total processing time to create a CNF sheet with a thickness of				
processing technique	0.28 mm	0.34 mm	0.42 mm	0.55 mm	1.65 mm
wet stacking lamination plus hot pressing (126 °C)	~1 h	1–2 h	1–2 h	1–2 h	6–7 h
vacuum filtering plus hot drying (90 °C)[14]	3–4 h	4–5 h	5–6 h	6–7 h	20–21 h
solution casting (23 °C)	~1 week	N/A	N/A	N/A	N/A

DOI: 10.1021/acsapm.9b00635
ACS Appl. Polym. Mater. 2019, 1, 2525–2534

reported in the literature. The time reported includes preparation, filtration, and drying time. Solution casting could not produce structures with a thickness greater than 0.28 mm without excessive wrinkling and warping.

The prepared CNF sheets in this work had some degree of translucency and flexibility, both of which significantly decreased as the number of layers increased (Figure 1a). Additionally, the sheets were flat and smooth to the touch even though the filtering mesh did impart small scale texturing to the surface which was identical to the crosshatched pattern of the woven metal filtering mesh (Figure 2c,d). SEM analysis of

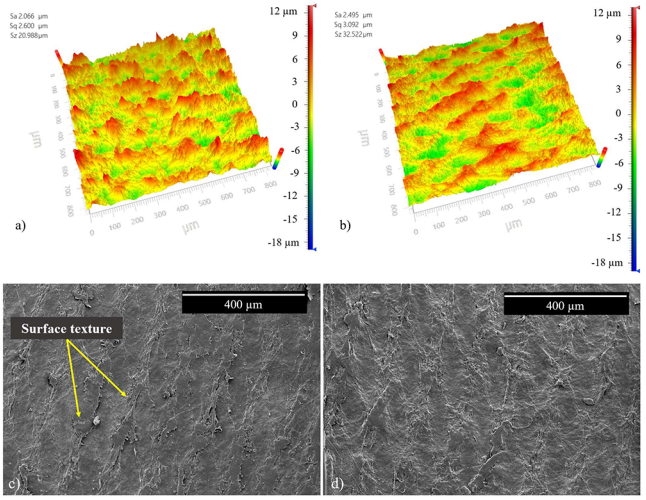

Figure 2. Optical profilometry (10×) of (a) a single-layer (~85 μm thick) and (b) an 8-layer (~547 μm thick) CNF sheet. (c) Surface texture imprint from the woven metal meshes onto a 1-layer pressed CNF sheet and (d) an 8-layer sheet. The surface roughness does not change significantly as the sheet thickness increase from 1 layer (Sq = 2.599 μm) to 8 layers (Sq = 3.092 μm).

the surface showed that this type of texturing imprint was also seen for the 2- and 6-layer sheets and is assumed to be present in the 3-, 4-, and 5-layer sheets (Figure S5). Furthermore, optical profilometry confirmed that the surface roughness did not change significantly (Sq = 2.6 μm versus Sq = ~3.1 μm) as the thickness increased from 85 to 547 μm (Figure 2a,b). This means that surface defects are not being generated as thickness increases and surface quality remains the same.

Cross-Sectional Surface Analysis. Water retention within the layers was very important throughout this process as it is well-known that removing water from cellulose slurries causes irreversible structural changes through heavy aggregation also known as hornification.[20,21,23] In this case, the wet CNF layers retained a significant amount of water (~90 wt %), which should have deterred the formation of a greater number of fibril−fibril hydrogen bonds or aggregates. Thus, when wet CNF layers are stacked and hot pressed together, hydrogen bonding can occur between them, and the layers consolidate to form a single sheet with no discernible interfaces. The entire cross section of CNF specimens composed of 1, 2, 4, 6, and 8 layers were analyzed with SEM to check for possible defects between the pressed layers. Defects could have resulted from incomplete contact between layers as a result of surface roughness/texture brought by the woven filtering mesh[24] (Figure 3). Unfortunately, laser cutting caused significant damage to the cut surface (e.g., melting, etc.), which extends ~10 μm into the bulk of the sample (Figure S6). As a result,

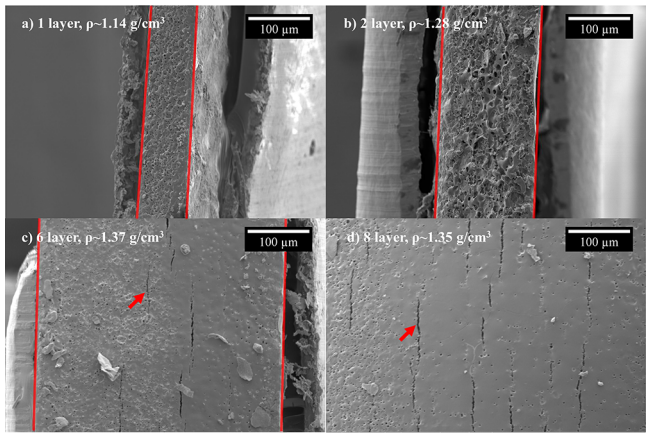

Figure 3. Cross-sectional SEM microphotography of (a) 1-layer sheet, (b) 2-layer sheet, (c) 6-layer sheet, and (d) 8-layer sheet with their respective densities. The density values shown are for the specific specimen analyzed. The red arrow highlights one of the flat defects while the red lines highlight the edges of the given sheet.

the cross-section surface was full of pinhole porosity and flat defects (Figure 3). For the thicker sheets (6 and 8 layers), flat defects are clearer and run parallel to the sheet stacking. At this early stage it is unclear whether these flat defects are associated at the layer−layer interface (Figure 3c,d and Figures S7−S9) as they appear throughout the cross section.

It is well-known that there exists a nanoporous network present in all neat CNF films.[3,25] In this case the porosity's magnitude or size must have decreased as the thickness of the sheets increased. This could explain the increase in density experienced by the 3-, 4-, 5-, 6-, and 8-layer sheets when compared to the 1- and 2-layer specimens. Table S1 shows a complete summary of the average density values for all CNF sheet thicknesses probed in this study

Thickness and Pressing Time Effect on the Mechanical Properties of CNF Sheets. Based on the statistical difference between data sets for different thicknesses (t test with 95% confidence interval), mechanical tensile testing showed that as the sheet thickness increased from 85 ± 2 μm (1 layer) to 153 ± 4 μm (2 layers), the ultimate strength increased from 151.8 ± 8.7 to 195.5 ± 1.9 MPa. The strength then remained constant at roughly 207 ± 2.5 MPa for thicker sheets (3, 4, 5, and 6 layers) (Figure 4a). Moreover, for all the sheets produced (1−8 layers), the ultimate strength results are significantly higher than that of the two different comparison baselines used (80 μm thick solution cast film and a 1-layer loosely constrained (~0 MPa) hot pressed sheet) which should carry the base mechanical properties of the most popular methods of making CNF films (cast and hot pressing). Other authors have shown similar trends for films prepared from bamboo CNF, where there was an initial increase in strength (~125 to 175 MPa) and then a plateau for thicker specimens (up to 205.5 μm).[26] For the 547 ± 29 μm thick sheets (8-layer), the strength decreased slightly to 184.8 ± 10.9 MPa. It is also interesting to note that the effective layer thickness decreased as the number of layers increased. For example, for the 1-layer sheet the effective layer thickness was ~85 μm/layer while for the 8-layer sheet it was ~68 μm/layer These differences may be a result of the compression of surface roughness on each layer during hot pressing (step 4, Figure S2). Table S1 lists all the measured average values relating to

DOI: 10.1021/acsapm.9b00635
ACS Appl. Polym. Mater. 2019, 1, 2525−2534

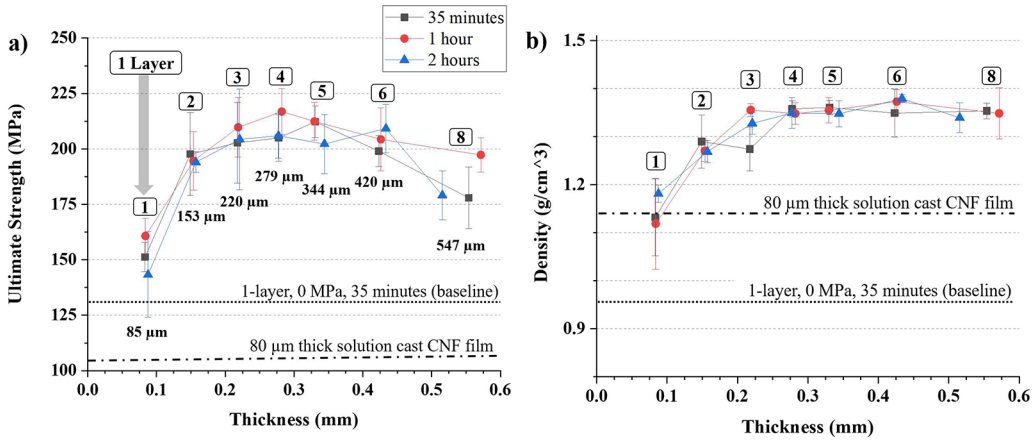

Figure 4. Scatter plot of (a) ultimate strength versus thickness and (b) density versus thickness for pure CNF sheets ranging from 1 to 8 layers thick for 35 min, 1 h, and 2 h press time. All the sheets were hot pressed at 0.36 MPa and 126 °C. The numbers shown above and below the curves represent the numbers of layers and the average sheet thickness for all pressing times. The baseline represents a single CNF layer processed at a pressure of 0 MPa and a temperature of 126 °C for 35 min. The second dashed line represents an 80 μm thick CNF solution-cast film.

the tensile mechanical performance of the produced CNF sheets.

To gain a better assessment of the mechanical properties of the produced sheets, the empirical relationship between ultimate strength and fibril diameter was used. This relationship was reported in the work done by Zhu et al.[27] In this study, the obtained ultimate strength values were on average 207 ± 2.5 MPa. These values were above the empirically found maximum possible for CNF films made with mean fibril diameters of 38 nm, which is estimated to be ∼162.2 MPa.[27] This approximation is made by taking the inverse of the square of the mean fibril diameter (Figure S1 and eq S1). The deviation from the empirical relationship was directly related to an increase in density with sheet thickness, following the same trend seen for ultimate strength (Figure 4b). For example. 3-, 4-, 5-, 6-, and 8-layer sheets with a thickness >153 μm had average higher densities in the range of 1.35 ± 0.02 g/cm^3, while 1- and 2-layer sheets had a density of 1.14 ± 0.03 and 1.28 ± 0.01 g/cm^3 (Table S1). To assess the strength−density relationship, a plot of ultimate strength versus density was made (Figure 5), and a linear fit to the results showed an R^2 = 0.968, demonstrating a strong correlation between the two variables. Though not explicitly stated, the increase in density with sheet thickness and its correlation with the ultimate strength were also reported by other authors.[17]

Pressing times were investigated to assess effect on sheet strength, in which longer pressing times would allow for more complete water removal and web consolidation, resulting in higher sheet densities (Figure 4b) and thus higher sheet strength (Figure 4a). For the 1−6-layer sheets longer pressing times did not affect the density or the tensile strengths. In contrast, the 8-layer sheet was influenced by pressing time where pressing for 1 h developed a higher strength (197.3 ± 7.7 MPa), which was above the 35 min case (177.9 ± 13.9 MPa) and the 2 h case (179.1 ± 11.0 MPa). The decrease in strength experienced by the 8-layer sheets was likely generated during sheet processing, a result of having a greater volume or mass of water being pressed together and removed from the structure. When the stacked wet structure was pressed, the CNF layers started sliding out of the mold (Figure S10). The mass movement likely formed different aggregates within the sheet, which after full consolidation of the web developed into

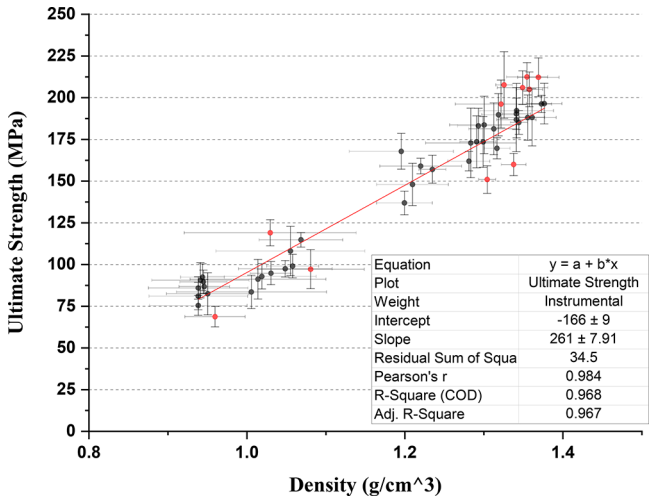

Figure 5. Ultimate strength versus density of CNF sheets. A linear regression model was fitted to the data. Residual analysis was utilized to remove any outliers which are highlighted in red. Data points with a standardized residual above or below ±10 STD were excluded from the linear fit.

weaker sites where failure is more likely to occur. Furthermore, the movement of CNF when pressing will usually manifest as a slightly rougher sheet surface, which was observed in all 8-layer sheets. A solution to this is to apply slow and controlled pressing to more slowly compress the layers as the water evaporates. Additionally, the density of all the specimens was not affected and remained statistically equivalent between all pressing times; hence, water was not likely retained within the thicker specimens.

For sheets with 1, 2, 3, 4, 5, and 6 layers the tensile elastic modulus remained constant at around 11.0 ± 0.9 GPa and decreased to 8.86 ± 0.3 GPa for the 8-layer sheets for all pressing times. The modulus for all sheets (e.g., hot pressed, constrained drying) was slightly lower than that of the baseline (1-layer, ∼0 MPa loosely constrained drying) with a modulus of 12.6 ± 0.8 GPa, yet equivalent to that of the 80 ± 3 μm thick solution cast CNF film (11.04 ± 1.7 GPa) (Figure 6a). Overall, the values obtained for the sheets (1−6 layers) were equivalent to what other authors have obtained for thin

DOI: 10.1021/acsapm.9b00635
ACS Appl. Polym. Mater. 2019, 1, 2525−2534

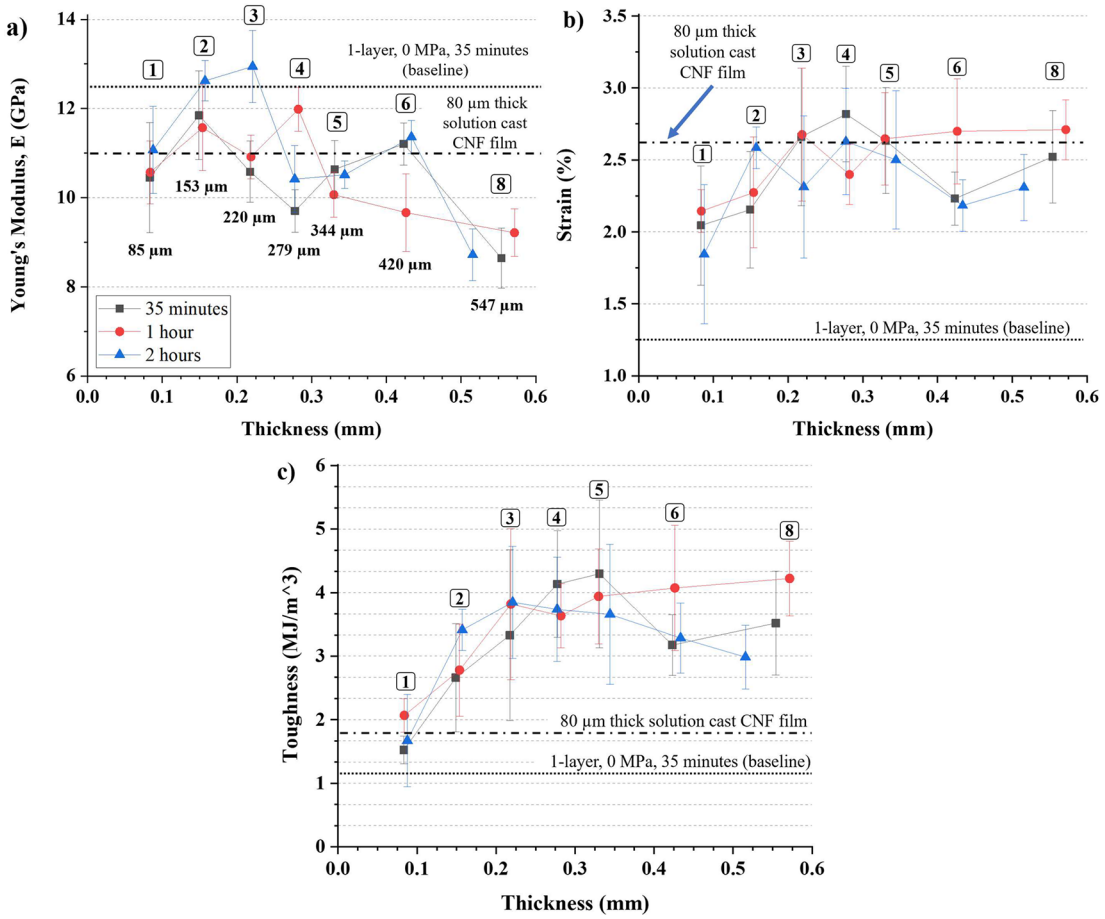

Figure 6. Scatter plot of (a) Young's modulus versus thickness, (b) strain versus thickness, and (c) toughness versus thickness for 35 min, 1 h, and 2 h press time. All the sheets were hot pressed at 0.36 MPa and 126 °C. The baseline represents a single CNF layer processed at a pressure of 0 MPa and a temperature of 126 °C for 35 min. The second dashed line represents an 80 μm thick CNF solution-cast film.

solution cast and pressed-dry CNF films.[28−30] The higher modulus obtained for the baseline (loosely constrained (~0 MPa) 1-layer sheet) was unexpected as it did not possess noticeable fibrillar alignment, which could have led to a higher modulus, as verified by SEM of the surface (Figure S11).[30,31] In contrast, there was a slight decrease in modulus seen for the 8-layer sheets, as compared to the thinner sheets (1−6 layers), which could possibly result from the formation of defects and nonbonded sites throughout the laminated structure or slippage at the grip sections during tensile testing due to the increase of load required to test the thicker specimens. Moreover, other authors have shown that constrained drying (i.e., hot pressing) does not have an effect on the elastic modulus.[31] When comparing between the different pressing times there appears to be no statistical difference for the elastic modulus between specimens with 1, 2, 5, and 8 layers. The exceptions were the 3-layer/2-h case that was higher than the 35 min and 1 h, the 6-layer/1-h case that was lower than that of the 35 min and 2 h, and the 4-layer/1-h case that was higher than the other two pressing times.

For all pressing times, strain to failure increased from ~2.01 ± 0.15% for 1-layer sheets to a constant value of ~2.50 ± 0.21% for 2-, 3-, 4-, 5-, 6-, and 8-layer sheets, which was equivalent to that of the solution-cast CNF film (~80 μm thick) with a strain to failure of 2.58 ± 0.55% (Figure 6b). The increase in strain to failure for the 2−8-layer sheets could originate from the fact that the more efficiently packed fibrils (e.g., higher density sheets) utilize more of their active surface area and better distribute the load (e.g., effectively lowering stress concentrations within sample) or that the nonbonded sites within the multilayer sheets give more flexibility to the structure. These results also indicate that while constrained drying lowers strain to failure for 1-layer sheets, it can be recovered if the CNF structure is made thicker by adding more sheets. Furthermore, other authors have shown that CNF films with lower densities experienced greater axial strain variations over the specimen surface which could lead to early failure.[31] This phenomenon is likely due to higher porosity and defects which act as stress concentration zones and could explain why 1-layer specimens fail first. Conversely, lower strain variations and smaller porosity/defects experienced by thicker sheets (>1 layer) translate to a better distribution of the applied load which suppresses early crack initiation and failure. Upon comparison of different pressing times, there appears to be no statistical difference for the strain to failure between specimens with 1, 2, 3, 4, and 5 layers. The exceptions were for the 6- and 8-layer sheets where the 1 h pressing time resulted in higher strain to failure than the 35 min and 2 h pressing times. It is unclear why this is the case at this time.

Similarly for all pressing times, the apparent toughness (work of failure) of the sheets increased from 1.75 ± 0.28 MJ/m^3 (1 layer) to 3.53 ± 0.36 MJ/m^3 for sheets with more than 1 layer (Figure 6c). The increase is likely physically linked to the higher density and lower critical defect size in a similar manner

DOI: 10.1021/acsapm.9b00635
ACS Appl. Polym. Mater. 2019, 1, 2525−2534

to strength as it is known that toughness scales with strength in brittle materials from Griffith's energy criterion.[32] Upon comparison of different pressing times, there appears to be no statistical difference for the apparent toughness of the specimens with 1−5 layers. The exceptions were for the 6- and 8-layer sheets where the 1 h pressing time resulted in higher apparent toughness than the 35 min and 2 h pressing times. It is unclear why this is the case at this time.

Loading Rate Effect on Mechanical Properties of CNF Sheets. The loading rate at which the wet sheets are pressed is a crucial processing parameter that must be carefully monitored to avoid any mass movement before full web consolidation. Ideally, the loading rate is fast enough to keep the desired pressure on the surface of the sheet but not so much as to initiate any mass moment (i.e., over pressing). Achieving this balance becomes increasingly challenging as water evaporates from the CNF sheets at uncontrolled rates. This is especially true for multiple layer sheets as more water (90 wt % per layer) is essentially stacked together and over pressing is easily initiated which causes severe damage to the structure of the sheet (Figure S10). Two 4-layer sheets (279 μm thick) pressed at two different rates show how the sheet quality is affected (Figure 7). For the fast loading rate, an applied pressure of 0.36 MPa was reached within 20 s (Figure 7a) while for the slow pressed case it took 4 min (Figure 7b). A very bright light was applied to the back of the 20 s sheet to better view the in-bulk aggregates formed due to the mass movement and the formation of a nonhomogeneous structure. It is important to note that the CNF movement is suppressed at the center of the 20 s sheet while it increases at the edges which is typical for materials undergoing elongational flow and more specifically biaxial flow.[33] Optical profilometry captured the surface roughness of the fast pressed and slow pressed sheets at the center and edge (Figure 7c,d and Figure S12a,b).

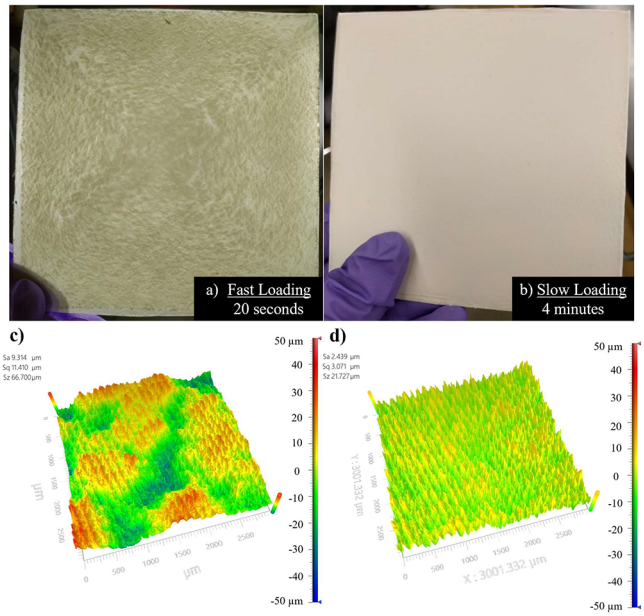

Figure 7. Photograph of 4-layer CNF sheets pressed at a fast loading rate (a) and slow loading rate (b) and optical profilometry (2.75×) of the center of the pressed sheets (c, d). Both sheets were pressed for 35 min at a temperature of 126 °C. The surface roughness at the center of the sheet increased significantly for the fast-pressed specimen (Sq = 11.410 μm vs Sq = 3.071 μm).

When the two sheets are compared, the roughness increased from ∼3.1 to ∼11.4 μm at the center and from ∼2.8 to ∼13 μm at the edge which confirms the excessive CNF movement and deformation caused in the bulk of the fast-pressed sheet.

Additionally, the results for three 4-layer sheets pressed at different rates show that the fastest loading rates lower the ultimate strength (Figure S13a). Similarly, the elastic modulus appears to decrease slightly as the loading rate is increased (Figure S13b). The decrease in mechanical properties at higher loading rates can be explained by the much greater surface roughness in the 20 s pressed sheet as compared to the 4 min specimen. The increase in surface roughness can be linked to a larger surface defect size that acts as larger critical stress concentration points and thus attains a lower ultimate strength as fracture will occur at a lower applied load.

Pressing Pressure Effect on the Mechanical Properties of CNF Sheets. Because of the strong correlation between strength and density (Figure 5), densification was desired; hence, higher pressing pressures of up to ∼5.17 MPa were probed. The results show that the strength started to decrease at pressures higher than 1.43 MPa (Figure S14a). Moreover, at higher pressures (5.17 MPa or greater) the rubber pads started deforming and impregnating the metal mesh which damaged the CNF sheets (Figure S15a). This caused the strength to decrease to a value of 124.3 ± 8.4 MPa. Loosely constrained (∼0 MPa) 4-layer samples showed the appearance of bubbles within the sheet; hence, some pressure is ultimately required to suppress bubbles and other defects like wrinkling (Figure S15b). It is important to note that the sheet defects heavily decreased the mechanical performance, yet the density was not affected until the pressure was above 3.59 MPa or below 0.36 MPa. For example, the 3.59 MPa specimens had a density of 1.34 ± 0.03 g/cm^3, which was equivalent to that of the loosely constrained (∼0 MPa) specimens (1.35 ± 0.08 g/cm^3) (Figure S14b). On the other hand, the ultimate strength of the 3.59 MPa specimens was 197.8 ± 7.3 MPa, which is higher than that of the loosely constrained (∼0 MPa) pressed samples (173.4 ± 8.55 MPa). The results also show that an applied pressure of 0.36 MPa is enough to develop the highest ultimate strength, and hence it was selected to process all previous hot-pressed sheets in the thickness study. Though densification at higher pressures was not achieved in this study, it may be possible if high pressure bearing rubber pads and meshes are used. Sample area can also be further reduced to increase pressure, yet fewer samples will be generated per sheet.

Fracture Surface Analysis of CNF Sheets. The fracture surface of the specimens was analyzed to gain a better understanding of the possible causes for early failure of the 1-layer sheets (i.e., lower strain %). As seen, the 1- and 2-layer specimens presented a fibrillar fracture surface with fibrils pointing in the loading direction which was identical to that of the 6- and 8-layer specimens (Figure 8). The fracture surfaces appear to have a layered structure which is similar to the fracture surfaces of CNF films prepared by other methods like solution casting as reported by other authors.[16] Because of the similarity between the fracture surfaces, there was no discernible influence of the presence of the layers or interfacial defects to cause early failure or lower strength values for thinner specimens. Hence, making the thicker specimens seems to conserve the fracture behavior, and no interlayer delamination is observed in the fracture zone.

DOI: 10.1021/acsapm.9b00635
ACS Appl. Polym. Mater. 2019, 1, 2525−2534

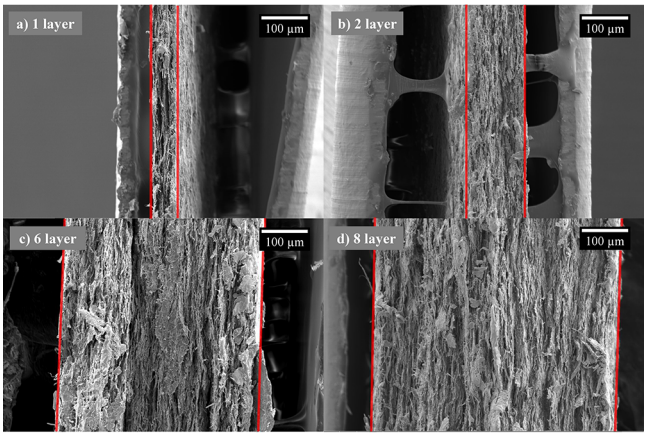

Figure 8. SEM microphotography of the fracture surface of (a) 1-layer, (b) 2-layer, (c) 6-layer, and (d) 8-layer dogbone specimens. As seen, all the specimens presented a paperlike fracture with fibrils pointing in the loading directions. The red lines highlight the analyzed fractured surface.

Benchmarking. Commodity polymers like poly(styrene) (PS) and nylon-6,6 and structural metal alloys like aluminum 2124 (T3) and aluminum 6061 (T6) were tested for comparison. Based on the thickness studies previously presented, a 4-layer CNF sheet was selected because the mechanical performance is assumed to be fully developed at this thickness. Table 2 compiles all the mechanical properties of the different materials studied. The results show that the CNF sheet is superior to PS and nylon-6,6 in both ultimate strength and elastic modulus. The opposite is true when the sheet is compared to Al 2024 and Al 6061. However, when the density of the materials is considered, as for specific strength, the results show that the CNF sheet is comparable to Al 2024 (T3). This means that CNF sheets are a strong lightweight material which could serve in structural applications. When looking at toughness, the results show that the CNF sheet was on average ~6.7 times tougher than PS. On the other hand, nylon-6,6, Al 2024, and Al 6061 had a toughness which was roughly 9, 11, and 6 times higher than that of the 4-layer CNF sheet (Table 2). The reduced toughness is linked to the small strain to failure seen for the CNF specimens which was expected due to the short nature of the CNF fibers as the mechanism for failure is fibrillar sliding and rupture.[16]

Although the direct comparison of CNF sheets to tempered aluminum alloys (2024 and 6061) showed inferior properties in terms of toughness, the extraction of CNF and its processing place a significantly lower burden on the environment. This is due to the extraction of bauxite which requires mining and its processing (Hall−Héroult process) which requires significant electrical energy (12.9−17.0 kWh/kg for aluminum vs 2.5 kWh/kg for CNF).[5,34] Additionally, the inherent sustainability of CNF holds a major advantage over tougher commodity polymers like nylon-6,6.

CONCLUSION

In this study, the fabrication of multilayered CNF sheets was assessed. The developed four-step process allowed for the creation of mechanically strong (ultimate strength = 207 ± 2.5 MPa), lightweight (ρ = 1.35 ± 0.02 g/cm^3), and tough (3.53 ± 0.36 MJ/m^3) pure CNF sheets in under 2 h. These sheets could serve in high-strength and low-density structural applications where aluminum alloys (2024 and 6061) and packing materials/containers where commodity polymers like poly(styrene) are currently used. A significant advantage of wet stacking lamination over conventional CNF film making techniques was found to be that it enabled the filtration through prestacked wet CNF layers rather than a thick CNF cake. Prestacked filtration avoided extending processing times; hence, a CNF sheet with a thickness of 1.65 ± 0.02 mm (24 layers) was made in under 7 h. Evaluation of the mechanical properties of the produced sheets showed that a plateau in ultimate strength of 207 ± 2.5 MPa was reached at a critical thickness between 85 ± 2 μm (1 layer) and 153 ± 4 μm (2 layers) for all pressing times investigated (35 min, 1 h, and 2 h). On the other hand, sheets with a thickness 547 ± 29 μm (8 layers) appeared to have a slightly lower mechanical performance possibly due to CNF movement during pressing. It is believed that the observed inferior mechanical behavior of thinner specimens (1-layer sheets) could be explained by the greater axial strain variations, larger porosity, and lower densities which lead to an early fracture. Additionally, loading rates greater than 2 min and pressing pressures of 0.36 MPa proved to be the optimal values to develop the highest possible mechanical properties. Moreover, this study demonstrated that sustainable and biofriendly nanosized polymers like CNF can be turned into larger structures with improved mechanical performance.

ASSOCIATED CONTENT

Supporting Information

The Supporting Information is available free of charge on the ACS Publications website at DOI: 10.1021/acsapm.9b00635.

Step-by-step images on the process of making CNF sheets, SEM images of the surface and cross-sectional area of the produced specimens, a TEM image of the CNF fibrils, the equation used to relate the ultimate strength of the sheets with the fibril diameter, box plots of the pressing rate and pressing pressure effect on the mechanical properties of the CNF sheets, images of CNF sheets with processing defects (PDF)

Table 2. Comparison of Measured Mechanical Properties of PS, Nylon-6,6, Al 2024, Al 6061, and CNF Sheets (4-Layer)[a]

material	density (g/cm^3)	ultimate strength (MPa)	Young's modulus (GPa)	strain to failure (%)	toughness (MJ/m^3)	specific strength	specific modulus	specific toughness
CNF sheet (4-layer)	1.35	209.2 ± 6.6	10.7 ± 1.2	2.61 ± 0.21	3.84 ± 0.3	154.96	7.93	2.84
poly(styrene)	1.05	10.9 ± 1.3	1.8 ± 0.02	4.53 ± 0.80	0.57 ± 0.13	10.38	1.71	0.54
nylon-6,6	1.31	44.9 ± 0.3	1.36 ± 0.08	74.5 ± 5.67	34.80 ± 1.85	34.27	1.04	26.56
Al 2024 (T3)	2.78	431.3 ± 29.6	58.5 ± 0.3	106 ± 2.82	41.55 ± 0.92	155.14	21.04	14.95
Al 6061 (T6)	2.7	254.3 ± 24.1	61.4 ± 2.3	7.57 ± 0.55	22.95 ± 1.1	94.19	22.74	8.50

[a]The units of specific strength, modulus, and toughness are MPa/(g/cm^3), GPa/(g/cm^3), and (MJ/m^3)/(g/cm^3).

DOI: 10.1021/acsapm.9b00635
ACS Appl. Polym. Mater. 2019, 1, 2525−2534

AUTHOR INFORMATION

Corresponding Author

*E-mail: jpyoungb@purdue.edu. Phone: +1 765-496-2294. Fax: +1 765 494-1204.

ORCID

Sami M. El Awad Azrak: 0000-0002-6384-7212
Caitlyn M. Clarkson: 0000-0001-9689-0842
Jeffrey P. Youngblood: 0000-0002-8720-8642

Funding

The authors thank the US Endowment and the Public-Private Partnership for Nanotechnology for funding this research (Grant 109217) and the National Science Foundation-Integrative Graduate Education and Research Traineeship: Sustainable Electronics (Grant 1144843).

Notes

The authors declare no competing financial interest.

ACKNOWLEDGMENTS

The authors thank Dr. Srinivasan Chandrasekar for making the optical profilometer equipment available and Mojib Sae for conducting and guiding the optical profilometry analysis and characterization.

REFERENCES

(1) Turbak, A. F.; Snyder, F. W.; Sandberg, K. R. Microfibrillated Cellulose, a New Cellulose Product: Properties, Uses, and Commercial Potential. *J. Appl. Polym. Sci.* **1983**, *37*, 815.

(2) Herrick, F. W.; Casebier, R. L.; Hamilton, J. K.; Sandberg, K. R. Microfibrillated Cellulose: Morphology and Accessibility. *J. Appl. Polym. Sci.* **1983**, *37*, 797.

(3) Moon, R. J.; Martini, A.; Nairn, J.; Simonsen, J.; Youngblood, J. Cellulose nanomaterials review: structure, properties and nanocomposites. *Chem. Soc. Rev.* **2011**, *40*, 3941.

(4) Saito, T.; Kimura, S.; Nishiyama, Y.; Isogai, A. Cellulose Nanofibers Prepared by TEMPO-Mediated Oxidation of Native Cellulose. *Biomacromolecules* **2007**, *8* (8), 2485−2491.

(5) de Assis, C. A.; Iglesias, M. C.; Bilodeau, M.; Johnson, D.; Phillips, R.; Peresin, M. S.; Bilek, E. M. T.; Rojas, O. J.; Venditti, R.; Gonzalez, R. Cellulose Micro- and Nanofibrils (CMNF) Manufacturing - Financial and Risk Assessment. *Biofuels, Bioprod. Biorefin.* **2018**, *12* (2), 251−264.

(6) Saito, T.; Nishiyama, Y.; Putaux, J. L.; Vignon, M.; Isogai, A. Homogeneous Suspensions of Individualized Microfibrils from TEMPO-Catalyzed Oxidation of Native Cellulose. *Biomacromolecules* **2006**, *7* (6), 1687−1691.

(7) Mascheroni, E.; Rampazzo, R.; Ortenzi, M. A.; Piva, G.; Bonetti, S.; Piergiovanni, L. Comparison of Cellulose Nanocrystals Obtained by Sulfuric Acid Hydrolysis and Ammonium Persulfate, to Be Used as Coating on Flexible Food-Packaging Materials. *Cellulose* **2016**, *23* (1), 779−793.

(8) Qiu, X.; Hu, S. Smart" Materials Based on Cellulose: A Review of the Preparations, Properties, and Applications. *Materials* **2013**, *6* (3), 738−781.

(9) Chowdhury, R. A.; Clarkson, C.; Youngblood, J. Continuous Roll-to-Roll Fabrication of Transparent Cellulose Nanocrystal (CNC) Coatings with Controlled Anisotropy. *Cellulose* **2018**, *25* (3), 1769−1781.

(10) Henriksson, M.; Berglund, L. A. Structure and Properties of Cellulose Nanocomposite Films Containing Melamine Formaldehyde. *J. Appl. Polym. Sci.* **2007**, *106*, 2817−2824.

(11) Chowdhury, R. A.; Clarkson, C.; Apalangya, V. A.; Islam, S. M. N.; Youngblood, J. P. Roll-to-Roll Fabrication of Cellulose Nanocrystal-Poly(Vinyl Alcohol) Composite Coatings with Controlled Anisotropy. *Cellulose* **2018**, *25* (11), 6547−6560.

(12) Peng, S. X.; Shrestha, S.; Yoo, Y.; Youngblood, J. P. Enhanced Dispersion and Properties of a Two-Component Epoxy Nanocomposite Using Surface Modified Cellulose Nanocrystals. *Polymer* **2017**, *112*, 359−368.

(13) Clarkson, C. M.; El Awad Azrak, S. M.; Chowdhury, R.; Shuvo, S. N.; Snyder, J.; Schueneman, G.; Ortalan, V.; Youngblood, J. P. Melt Spinning of Cellulose Nanofibril/Polylactic Acid (CNF/PLA) Composite Fibers For High Stiffness. *ACS Appl. Polym. Mater.* **2019**, DOI: 10.1021/acsapm.8b00030.

(14) Sehaqui, H.; Liu, A.; Zhou, Q.; Berglund, L. A. Fast Preparation Procedure for Large, Flat Cellulose and Cellulose/Inorganic Nanopaper Structures. *Biomacromolecules* **2010**, *11* (9), 2195−2198.

(15) Sehaqui, H.; Zhou, Q.; Ikkala, O.; Berglund, L. A. Strong and Tough Cellulose Nanopaper with High Specific Surface Area and Porosity. *Biomacromolecules* **2011**, *12*, 3638−3644.

(16) Henriksson, M.; Berglund, L. A.; Isaksson, P.; Lindström, T.; Nishino, T. Cellulose Nanopaper Structures of High Toughness Cellulose Nanopaper Structures of High Toughness. *Biomacromolecules* **2008**, *9* (6), 1579−1585.

(17) Syverud, K.; Stenius, P. Strength and Barrier Properties of MFC Films. *Cellulose* **2009**, *16* (1), 75−85.

(18) Chavan, P. A.; Shinde, B. S.; Bhagwat, V. N.; Shinde, P. P.; Patil, B. D. Pocket Ventilation System In Dryer Section Of Paper Machine: A Review. *Int. J. Technol. Enhanc. Emerg. Eng. Res.* **2015**, *3* (03), 11−14.

(19) Przybysz, P.; Dubowik, M.; Kucner, M. A.; Przybysz, K.; Buzała, K. P. Contribution of Hydrogen Bonds to Paper Strength Properties. *PLoS One* **2016**, *11* (5), e0155809.

(20) Ghosh, A. K. *Fundamentals of Paper Drying − Theory and Application from Industrial Perspective*; InTech: 2011.

(21) Weise, U. Characterization and Mechanism of Changes in Wood Pulp Fibres Caused by Water Removal. *Acta Polytech. Scand. Chem. Technol. Ser.* **1997**, No. 249.

(22) TAPPI. Forming Handsheets for Physical Tests of Pulp. Test Method TAPPI/ANSI T 205 Sp-18. *Tappi* **2002**, 1−9.

(23) Peng, Y.; Gardner, D. J.; Han, Y. Drying Cellulose Nanofibrils: In Search of a Suitable Method. *Cellulose* **2012**, *19* (1), 91−102.

(24) Cheng, W.; Dunn, P. F.; Brach, R. M. Surface roughness effects on microparticle adhesion. *J. Adhes.* **2002**, *78*, 929−965.

(25) Bardet, R.; Reverdy, C.; Belgacem, N.; Leirset, I.; Syverud, K.; Bardet, M.; Bras, J. Substitution of Nanoclay in High Gas Barrier Films of Cellulose Nanofibrils with Cellulose Nanocrystals and Thermal Treatment. *Cellulose* **2015**, *22* (2), 1227−1241.

(26) Zhang, X.; Yu, Y.; Jiang, Z.; Wang, H. Influence of Thickness and Moisture Content on the Mechanical Properties of Microfibrillated Cellulose (MFC) Films. *Wood Res.* **2016**, *61* (6), 851−860.

(27) Zhu, H.; Zhu, S.; Jia, Z.; Parvinian, S.; Li, Y.; Vaaland, O.; Hu, L.; Li, T. Anomalous Scaling Law of Strength and Toughness of Cellulose Nanopaper. *Proc. Natl. Acad. Sci. U. S. A.* **2015**, *112* (29), 8971−8976.

(28) Alcalá, M.; González, I.; Boufi, S.; Vilaseca, F.; Mutjé, P. All-Cellulose Composites from Unbleached Hardwood Kraft Pulp Reinforced with Nanofibrillated Cellulose. *Cellulose* **2013**, *20* (6), 2909−2921.

(29) Chun, S. J.; Lee, S. Y.; Doh, G. H.; Lee, S.; Kim, J. H. Preparation of Ultrastrength Nanopapers Using Cellulose Nanofibrils. *J. Ind. Eng. Chem.* **2011**, *17* (3), 521−526.

(30) González, I.; Alcalà, M.; Chinga-Carrasco, G.; Vilaseca, F.; Boufi, S.; Mutjé, P. From Paper to Nanopaper: Evolution of Mechanical and Physical Properties. *Cellulose* **2014**, *21* (4), 2599−2609.

(31) Kulachenko, A.; Denoyelle, T.; Galland, S.; Lindstrom, S. B. Elastic Properties of Cellulose Nanopaper. *Cellulose* **2012**, *19* (3), 793−807.

(32) Griffith, A. A. The Phenomena of Rupture and Flow in Solids. *Philos. Trans. R. Soc., A* **1921**, *221* (582-593), 163−198.

(33) Singh, A. P.; Rey, A. D. Computer Simulation of Dynamics and Morphology of Discotic Mesophases in Extensional Flows. *Liq. Cryst.* **1995**, *18* (2), 219−230.

DOI: 10.1021/acsapm.9b00635
ACS Appl. Polym. Mater. 2019, 1, 2525−2534

(34) Report, A. Alcoa Annual Report, 2017.

DOI: 10.1021/acsapm.9b00635
ACS Appl. Polym. Mater. 2019, 1, 2525−2534